Optik - International Journal for Light and Electron Optics 236 (2021) 166621

Contents lists available at ScienceDirect

Optik

journal homepage: www.elsevier.com/locate/ijleo

Original research article

Effect of intense laser and electric fields on nonlinear optical properties of cylindrical quantum dot with Morse potential

F. Ungan [a], M.K. Bahar [b], M.G. Barseghyan [c], L.M. Pérez [d,*], D. Laroze [d]

[a] Faculty of Technology, Department of Optical Engineering, Sivas Cumhuriyet University, 58140 Sivas, Turkey
[b] Faculty of Science, Department of Physics, Sivas Cumhuriyet University, 58140 Sivas, Turkey
[c] National University of Architecture and Construction of Armenia, Teryan 105, 0009 Yerevan, Armenia
[d] Instituto de Alta Investigación, CEDENNA, Universidad de Tarapacá, Casilla 7D, Arica, Chile

ARTICLE INFO

Keywords:
Nonlinear optical properties
Electric field
Laser field
Quantum dot

ABSTRACT

In this study, the influence of the external electric field on the nonlinear optical properties of a laser dressed cylindrical quantum dot with axial Morse potential are theoretically investigated using the total optical absorption coefficient as well as relative refractive index changes. The effect of the structural parameters on the structure's intraband optical properties is analyzed, optimizing the quantum dot in terms of the total optical absorption coefficient and the relative refractive index. Single-electron energies and wave functions of the system have been determined using analytical methods and the exact diagonalization technique. The quantities above mentioned are examined with the compact-density-matrix approach. The obtained results demonstrated that the system's intraband optical properties closely depend on both the applied external fields and the structural parameters. Such adequate tuning of the laser-dressed cylindrical quantum dots' intraband optical properties gives us new possibilities in the regions of interest for optoelectronic device applications.

1. Introduction

The optoelectronic devices applications of heterostructures such as quantum wires and quantum dots (QDs) have been developed in parallel due to advanced nano-fabrication technology. Encompassing optical effects in low-dimensional structures are more blatant compared to that of bulk materials [1]. The experimental and theoretical investigations of the QDs have attracted more attention in recent years because of their broad area of use [2–4]. Due to the possibility of production of QDs, including different geometry thanks to advanced nano-fabrication technology, the number of theoretical studies on QDs with various shape confinements has increased [5–8]. Theoretical investigations performed on QDs are more concentrated on the nonlinear optical rectification [9], the total refractive index changes (RICs) [10], the total absorption coefficients (ACs) [11], the second and third harmonic generation characteristics [12], the effect of hydrostatic pressure on physical characteristics [13] and the external field examinations [14]. The optical ACs and the optical RICs of a spherical QD with parabolic confinement under the influence of the external electric field have been investigated in the framework of a perturbative approach [15]. The effects of the lateral external electric field applied on an exciton encompassed in a single InGaN QD have been studied using the micro-photoluminescence spectroscopy, determining that the electric field forms a blatant shift on exciton energy [16]. The nonlinear optical rectification characteristics of a parabolic QD under the

* Corresponding author.
E-mail address: lperez@uta.cl (L.M. Pérez).

https://doi.org/10.1016/j.ijleo.2021.166621
Received 11 September 2020; Received in revised form 3 February 2021; Accepted 22 February 2021
Available online 4 March 2021
0030-4026/© 2021 Elsevier GmbH. All rights reserved.

influence of the external electric and magnetic fields has been analyzed theoretically within the framework of an iterative method [17]. The second and third harmonics generation characteristics of a cone-like QD have also been analyzed within an iterative method [18]. Let us remark that the external electric field drastically changes the system's optical characteristics, such as the RICs, the ACs, exciton energy, and optical rectification, by remodeling the confinement strength of the QD system. A similar tool can be the external magnetic field [19–21]. Besides the difference between the effect of the electric and magnetic fields, the magnetic field has been recently analyzed [22,23].

Another external field that has remarkable effects on the electronic and optical properties of QDs is the intense laser field (ILF). The ILF diverges from the electric and magnetic fields due to its ability to disrupt the system's symmetry and thus gain the second harmonics generation characteristic to the related semiconductor low-dimensional system. In a nutshell, the external electric and magnetic fields lead to remarkable results in optical features by modifying the confinement effects of QDs. The influences of the electric and magnetic fields on systems can be different for QDs with different confinements. Such differences and the alternativeness of the external electric and magnetic field, due to its time-dependent and high-frequency, make rigorous theoretical investigations with the ILF stand out when compared to ones in other fields. The effect of the ILF on donor impurities of a spherical QD confined by infinity barrier potential has been viewed using the numerical integration Schrödinger equation [24]. The optical RICs and ACs [25], the second and third harmonics generation characteristics [26], and the nonlinear optical rectification characteristics [27] are some of the important theoretical research subjects that consider effects of the ILF. It is essential to know the alternative of the structure parameters in terms of the ILF's effect on the related observable, as well as in the electric and magnetic fields. In this sense, it is the first step to examine the ILF's effect on the localization of the quantum system. Therefore, the effects of the potential parameters and the ILF parameter should be investigated, performing the alternative parameter analysis. Such analysis has been executed for laser-driven two-electron parabolic QD in plasmas [28], and two-electron pseudo-dot under the influence of the ILF in plasmas [29]. In these studies, it is understood that the ILF application can be an alternative to experimental arguments.

In the present study, the Morse potential is considered for QD confinement potential [30]. This potential was chosen because it can be produced thanks to advanced nanofabrication techniques and has a well-like structure in accordance with experimental prediction [33]. Cylindrical confinement with a particular diameter was taken into consideration in order to restrict the electron mobility in the quantum system. The electron quantization was provided by performing axial growth (Morse-type) at a specific axis (z-axis). In the present study, the primary motivation is to probe the combined influences of structural parameters (CQD radius and Morse potential parameters) and the external fields (the electric field and ILF) on the ACs and RICs of CQD. In this analysis, we work to find out the alternativeness to each of the structural parameters and the external field parameters on the RICs and ACs. Thus, we aim to determine optimum CQD conditions with Morse confinement potential in terms of the optical RICs and ACs to obtain banausic data in possible technological applications of such CQD. The manuscript is organized as follows: In Section 2, the theoretical model and method are introduced for the optical responses. In Section 3, obtained results and their analysis are provided. Finally, a brief summary of the obtained results and the examination of the alternativeness of parameters on observables is given in Section 4.

2. Theory

We consider three dimensional CQD containing a single electron. As an axial potential is chosen one-dimensional Morse potential, however as a lateral confinement potential, we choose the model of finite square well. In cylindrical coordinates, the Hamiltonian of an electron confined in this structure under the influence of EF applied in parallel to the growth direction (z) of the structure (without ILF effects) can be written as follows [1]

$$\widehat{H} = -\frac{\hbar^2}{2m^*}\left(\frac{\partial^2}{\partial\rho^2}+\frac{1}{\rho}\frac{\partial}{\partial\rho}+\frac{1}{\rho^2}\frac{\partial^2}{\partial\phi^2}\right) + V_\rho(\rho) - \frac{\hbar^2}{2m^*}\frac{\partial^2}{\partial z^2} + V_M(z) + |e|\mathrm{Fz}, \tag{1}$$

where m^* is the effective mass of the electron, e is the charge of the electron, F is the electric field strength, $\rho = \sqrt{x^2+y^2}$, $V_M(z)$ and $V(\rho)$ are the confinement potentials in the z-direction and in the $(x-y)$ plane, respectively. The expressions for the potential can be explicitly given by [30–32]

$$V_M(z) = V_0(e^{-2\eta z} - 2e^{-\eta z}), \tag{2}$$

and

$$V_\rho(\rho) = \begin{cases} 0, & \rho \le R \\ V_0, & \rho > R \end{cases} \tag{3}$$

Here, $V_0 = 0.6(1.155x + 0.37x^2)$ eV is the height of the barrier potential, and η determines the effective length of QW. Moreover, with the increment of η the effective length of the QW decreases. R is the QD radius, and x is the aluminum concentration [34]. Throughout the present study, the height of the barrier potential is taken as $V_0(x = 0.3) = 228$ meV. Assuming that polarization of the laser field is parallel to the z-direction, the dressed Morse confinement potential takes the following form [35–37]

$$V_M(z,\alpha_0) = \frac{\Omega}{2\pi}\int_0^{2\pi/\Omega} V_M(z+\alpha_0 sin\Omega t)\mathrm{d}t, \tag{4}$$

where $\alpha_0 = eA_0/m^*\Omega$ is the ILF parameter, A_0 describes the field strength and Ω is the angular frequency of the incident laser. The analytical expression for the dressed potential can be written as

$$V_M(z,\alpha_0) = V_0\left(e^{-2\eta z}I_0(2\eta\alpha_0) - 2e^{-\eta z}I_0(\eta\alpha_0)\right), \tag{5}$$

where $I_0(x)$ is the modified Bessel function of the first kind.

In order to show the effect of the potential parameter and ILF effects on the Morse confinement potential, in Fig. 1 we present the variation of the shape of potential for different values of η, and α_0. An increase in the η parameter leads to a decrease in the effective well width. Moreover, we see that the minimum point of the potential shifts to higher values of z and scales linearly with α_0. On the other hand, we remark that when the ILF parameter increases, the confinement potential becomes highly anharmonic.

On the other hand, the total eigenfunction can be expressed as $\Psi(\rho,z) = N\varphi(\rho)\psi(z)$, where N is the normalization constant, and $\varphi(\rho)$ and $\psi(z)$ are the wave functions for coordinates ρ and z, respectively. The total energy eigenvalue of CQD can be written as $E = E_\rho + E_z$. Therefore, the corresponding two-dimensional (lateral direction) Schrödinger equation for the confined motion of the electron in the $(x-y)$ plane is

$$\left[-\frac{\hbar^2}{2m^*}\left(\frac{\partial^2}{\partial\rho^2}+\frac{1}{\rho}\frac{\partial}{\partial\rho}+\frac{1}{\rho^2}\frac{\partial^2}{\partial\phi^2}\right)+V_\rho(\rho)\right]\varphi(\rho) = E_\rho\varphi(\rho), \tag{6}$$

with the solution of the form [38,39]

$$\varphi(\rho) = \begin{cases} N_1 J_0(r_{10}\rho), & \rho \le R \\ N_1\dfrac{J_0(r_{10}R)}{K_0(b_{10}R)}K_0(b_{10}\rho), & \rho > R \end{cases} \tag{7}$$

where N_1 is the normalization constant, J_0 and K_0 are modified Bessel functions of 0th order, $r_{10} = \sqrt{2m^*E_\rho/\hbar^2}$ and $b_{10} = \sqrt{2m^*V_0/\hbar^2 - r_{10}^2}$. The energy eigenvalue E_ρ is determined by using the continuity of the wave function and its first derivative at $\rho = R$. On the other hand, the bound electron energy levels in a Morse confinement potential under the EF and non-resonant ILF can be obtained via the solution of the following time-independent one-dimensional Schrödinger equation:

$$\left[-\frac{\hbar^2}{2m^*}\frac{\partial^2}{\partial z^2} + V_M(z,\alpha_0) + |e|\mathrm{Fz}\right]\psi(z) = E_z\psi(z). \tag{8}$$

For this equation, in order to obtain the energy levels and the corresponding wave functions, we use the standard diagonalization technique [40]. After obtaining the total energy and the corresponding eigenfunctions of the electron, we use the analytical expressions for the total absorption coefficient and the relative refractive index change [41]. Taking into account the linear and first nonlinear contribution, they can respectively be written as $\beta(\omega,I) = \beta^{(1)}(\omega) + \beta^{(3)}(\omega,I)$ and $\Delta n(\omega,I) = \Delta n^{(1)} + \Delta n^{(3)}(\omega,I)$, such that [42,43]

$$\beta^{(1)}(\omega) = \omega\sqrt{\frac{\mu}{\varepsilon_0}}\,\frac{|M_{10}|^2\sigma_v\hbar\Gamma_0}{(E_{10}-\hbar\omega)^2+(\hbar\Gamma_0)^2}, \tag{9}$$

$$\beta^{(3)}(\omega,I) = -\frac{2I\omega}{\varepsilon_0 n_r c}\sqrt{\frac{\mu}{\varepsilon_R}}\,\frac{|M_{10}|^4\sigma_v\hbar\Gamma_0}{\left[(E_{10}-\hbar\omega)^2+(\hbar\Gamma_{10})^2\right]^2}\left(1-\frac{|\delta M|^2}{|2M_{10}|^2}\,\frac{(E_{10}-\hbar\omega)^2-(\hbar\Gamma_0)^2+2(E_{10})(E_{10}-\hbar\omega)}{(E_{10})^2+(\hbar\Gamma_0)^2}\right), \tag{10}$$

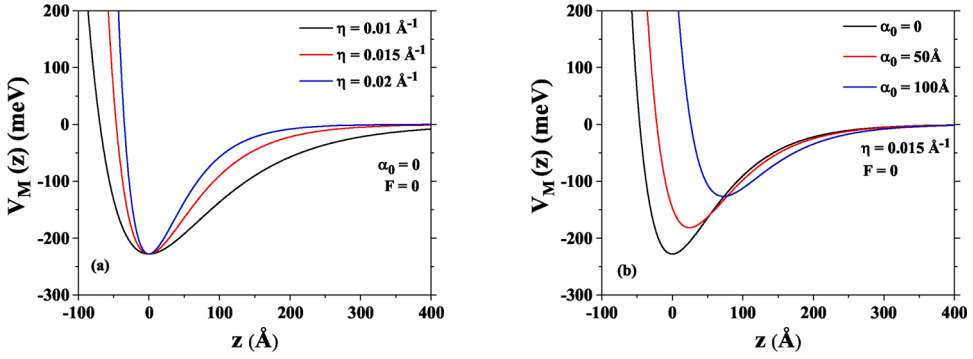


Fig. 1. Axial Morse potential for CQD as a function of coordinate z. (a) Dependence with different values of η at $\alpha_0 = 0$. (b) Dependence with different values of α_0 at $\eta = 0.015$ Å^{-1}. In both cases $V_0 = 228$ meV and the electric field is zero, $F = 0$.

$$\frac{\Delta n^{(1)}(\omega)}{n_r} = \frac{\sigma_v |M_{10}|^2}{2n_r^2 \varepsilon_0} \left(\frac{E_{10} - \hbar\omega}{(E_{10} - \hbar\omega)^2 + (\hbar\Gamma_0)^2} \right), \tag{11}$$

$$\begin{aligned} \frac{\Delta n^{(3)}(\omega, I)}{n_r} &= -\frac{\mu c |M_{10}|^2}{4n_r^3 \varepsilon_0} \frac{\sigma_v I}{\left[(E_{10} - \hbar\omega)^2 + (\hbar\Gamma_0)^2\right]^2} \\ &\times \left[4(E_{10} - \hbar\omega)|M_{10}|^2 - \frac{|\delta M|^2}{\delta\Gamma_{10}} \left((E_{10} - \hbar\omega)[E_{10}(E_{10} - \hbar\omega) - (\hbar\Gamma_0)^2] - (\hbar\Gamma_0)^2(2E_{10} - \hbar\omega) \right) \right] \end{aligned} \tag{12}$$

Here, (ω, I) are the angular frequency and the electromagnetic field intensity of incident light, $M_{ij} = |\langle\psi_i|\mathrm{e}\ z|\psi_j\rangle|$ is the matrix element of the electric dipole moment, σ_v is the electron density in a CQD, μ is the permeability of the system, ε_0 is the free space dielectric constant, n_r is the refractive index, ε_R is the real part of the permittivity, c is the velocity of light in the vacuum, and $\Gamma_0 = 1/\tau_{10}$ indicates the relaxation rate of the final and initial states. Also, we have used the following notation: $E_{10} = E_1 - E_0$, $\delta M = M_{11} - M_{00}$ and $\delta\Gamma_{10} = (E_{10})^2 + (\hbar\Gamma_0)^2$. In the next section numerical simulations of these indicators are performed.

3. Results and discussion

Let us present numerical results of the effect of the external electric field and intense laser field on the total absorption coefficient and the relative refractive index change in a cylindrical quantum dot with Morse axial potential confinement. In our calculations the parameters corresponding to GaAs are, $m^* = 0.067m_0$ (m_0 is the single electron bare mass), $e = 1.602 \times 10^{-19}$ C, $\hbar = 1.056 \times 10^{-19}$ J s, $\varepsilon_0 = 8.854 \times 10^{-12}$ C^2/N m^2, $\sigma_v = 3.0 \times 10^{22}$ m^{-3}, $V_0 = 228$ meV, $\tau_{10} = 0.14$ ps.

It is worth to note that the QD with Morse confinement potential conforms with experimental predictions due to its parabolic potential encompassing profile [33]. We investigate the effects on relative RICs and total ACs of four different parameters: (η, R) concerning the potential confinement parameters, and (F, α_0) regarding the external fields. Fig. 2 shows the change of the energy gap between two bound states with the lowest energy as well as the M_{10} matrix elements as a function of confinement potential parameters. The increase of η parameter enhances the energy gap between the ground and first excited states, as it is shown in panel (a) of Fig. 2. Note that the increment of η provides a more repulsive potential by decreasing the encompassing strength. Then, this repulsiveness pushes the localizations to higher energy levels—the augmentation of QD repulsiveness due to increasing η causes the decrease of M_{10} matrix elements. On the other hand, the effect of the radius R is opposite to η, as can be observed in panel (b) of Fig. 2. Indeed, the energy difference decreases as R increases, whereas the M_{10} matrix elements increase with R. Although the encompassing capacity increases in a larger QD, the localizations get shallow, while the corresponding energy gap between ground and first excited states decreases.

The panels (a) and (b) of Fig. 3 show the change of the energy gap between two bound states with the lowest energy as well as the M_{10} matrix elements as a function of the external field parameters F and α_0, respectively. In panel (a), we can clearly observe that the increase in the electric field strength enhances the energy gap, whereas in panel (b) the energy gap decreases as the laser field strength α_0 increases. Therefore, these effects are opposed to each other. This behavior of the energy gaps are caused by the corresponding changes in energy levels of ground and first excited states. Similar antagonism effects have been observed in the case of a single quantum ring [35].

Figs. 4 and 5 display the total absorption coefficient, β, as a function of the incident photon energy for different values of the control parameters. In particular, Fig. 4 shows the effect of the geometric parameters, while the external fields' influence is presented in Fig. 5. Figure 4 shows that, with the increment of η, the blue shift is observed in the total absorption spectrum, while the redshift is observed with an increment of R. Additionally, it is worth noting that the absorption intensities are weakening. These results are in agreement with the corresponding behaviors of the energy gaps and matrix elements. The blue and redshifts in the absorption spectrum have been observed in Fig. 5 by changing the electric field strength and ILF parameter. We remark that these effects are given by the corresponding changes on the energy gaps.

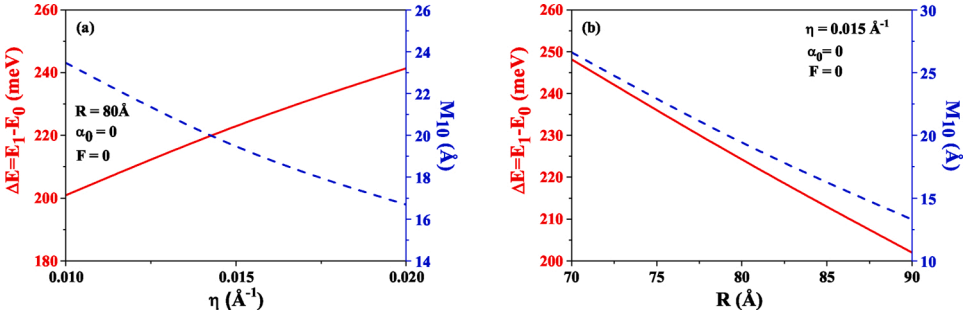


Fig. 2. The change of the energy gap between two bound states with the lowest energy and M_{10} matrix elements as a function of the control parameters. (a) Here, η is varied, while the rest of the parameters are fixed. (b) Here, R is varied, while the rest of the parameters are fixed.

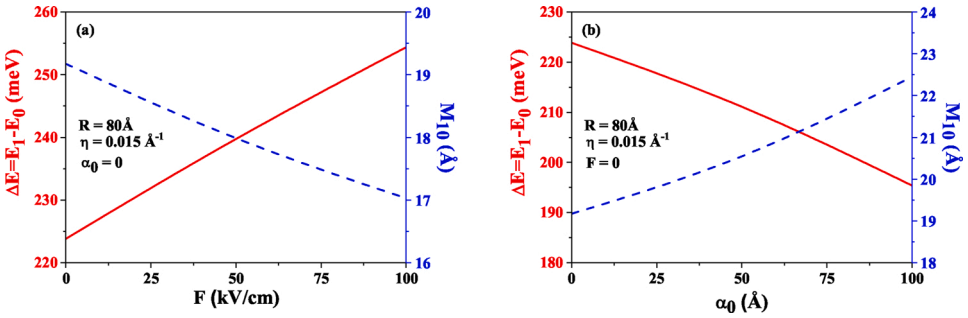


Fig. 3. The change of the energy gap between two bound states with the lowest energy and M_{10} matrix elements as a function of the control parameters. (a) Here, F is varied, while the rest of the parameters are fixed. (b) Here, α_0 is varied, while the rest of the parameters are fixed.

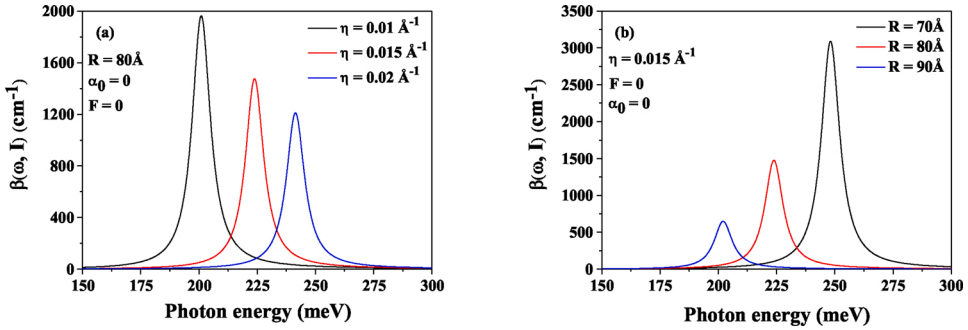


Fig. 4. Total absorption coefficient, β, as a function of incident photon energy for different values of the parameters. (a) Here, R is fixed and η is varied: $\eta = (0.01, 0.015, 0.02)$ cm^{-1}. (b) Here, η is fixed and R is varied: $R = (70, 80, 90)$ Å.

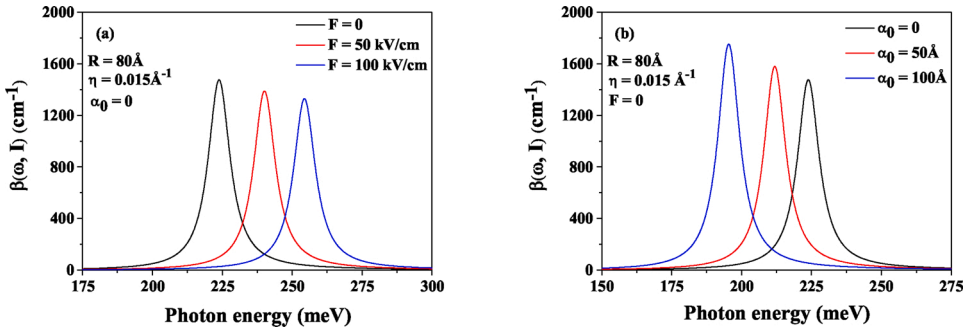


Fig. 5. Total absorption coefficient, β, as a function of incident photon energy for different values of the parameters. (a) Here, α_0 is fixed and $F \in (0, 50, 100)$ kV/cm. (b) Here, F is fixed and $\alpha_0 \in (0, 50, 100)$ Å.

Figs. 6 and 7 present the behavior of the relative refractive index change, $\Delta n/n_r$, as function of incident photon energy for different values of the control parameters. In panel (a) of Fig. 6, the outcome of η on relative RIC is shown. As the augment of η decreases the encompassing strength, the rising of the localizations as a result of increasing E_{10}, a blue-shift is observed in the RIC resonant frequency. In addition, the increment of η reduces relative RIC amplitudes due to the decrease of M_{10} matrix elements. On the other hand, a red-shift is expected at relative RIC resonant frequencies when the radius is increased. These frequencies come closer to each other as it is observed in panel (b) of Fig. 6. We remark that when M_{10} matrix elements in a larger QD are smaller, relative RIC amplitudes will also be smaller.

Panel (a) of Fig. 7 shows that an increment on F shifts to blue the RRIC resonant frequencies. This happens because larger values of F lead to an increment in the energy gap, E_{10}. Similarly, due to M_{10} decreases when the field strength increases, the relative refractive index amplitudes also decreases. Finally, $\Delta n/n_r$ is complementary to F and α_0 as it shown in panel (b) of Fig. 7.

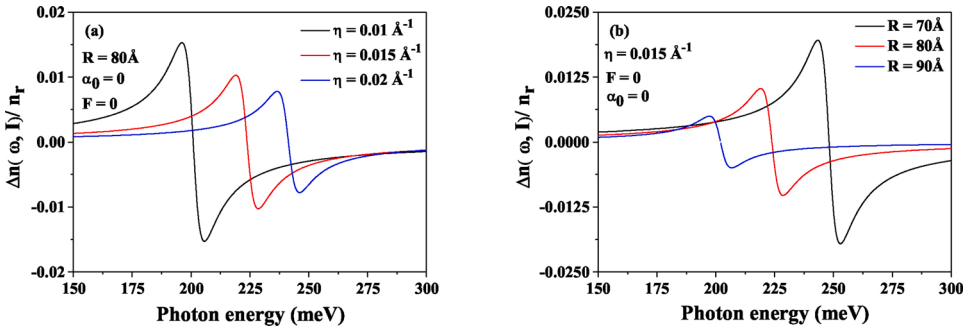


Fig. 6. Relative refractive index change, $\Delta n/n_r$ as a function of incident photon energy for different values of the parameters. (a) Here, R is fixed and $\eta \in (0.01, 0.015, 0.02)$ cm^{-1}. (b) Here, η is fixed and $R \in (70, 80, 90)$ Å.

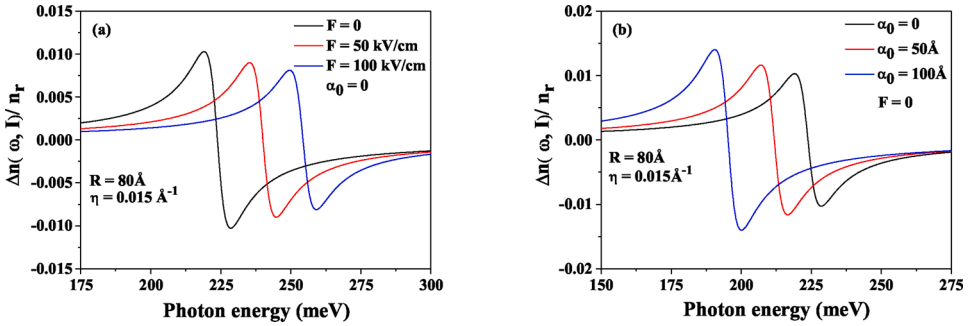


Fig. 7. Relative refractive index change, $\Delta n/n_r$ as a function of incident photon energy for different values of the parameters. (a) Here, α_0 is fixed and $F \in (0, 50, 100)$ kV/cm. (b) Here, F is fixed $\alpha_0 \in (0, 50, 100)$ Å.

MNT_ELSEVIER_JOURNAL_IJLEO_166621_110

4. Conclusions

In this study, we have analyzed the effects of the external electric and the intense laser fields on optical properties in a CQD with axial Morse confinement potential. In particular, the absorption coefficient and relative refractive index change have been examined as a function of four control parameters: the geometric parameters (η, R), the electric field strength F, and the ILF parameter α_0. We have observed that the total absorption coefficient and relative refractive index change have been similarly affected by η, and F. Thus, the blue-shift resonant frequencies have been observed. The increase of α_0 and R has led to a red-shift in a total absorption coefficient and relative refractive index change under resonant frequencies. Thus, η and R are structure parameters of cylindrical symmetry, and experimental arguments require to change them. However, α_0 and F are more practical to implement. In this manner, η-F and α_0-R are complementary parameters. When considering behaviors of η and F on the amplitudes, it is understood that both of them decrease the amplitudes. However, the influence of η on the amplitudes is more dominant than that of F. In this case, it can be noted that CQD is more optimum at smaller values of η in terms of total absorption coefficient and relative refractive index change. However, considering F as an alternative to η is an important achievement in terms of practicality in the applicability of F. When considering decrement in total absorption coefficient and relative refractive index change amplitudes because of increasing R, it is clear that F is an alternative to η and R to adjust the optimum of CQD. In such alternativeness, while the most dominant parameter is η, the most feeble one is F. The ILF role on total absorption coefficient and relative refractive index change amplitudes is different from that of the structure parameters and the external electric field. The increment of ILF parameter α_0 the amplitudes increases. Here it is a very evident outcome that η, R, F, and α_0 are functional on the total absorption coefficient and relative refractive index change resonant frequencies of CQD, and there are blatant effects on the CQD structure. However, when taking into consideration the amplitudes, the structure parameters (η, R) are more dominant and functional compared to the external field parameters (F, α_0). Since the possibility of CQD production with axial Morse confinement potential, today's nano-fabrication technology is taken into account. We think that explanations done in this study determining optical characteristics using the structural parameters and the external fields can be important for experimental research and technological applications.

Conflict of interest

None declared.

Declaration of Competing Interest

The authors report no declarations of interest.

Acknowledgments

Our thanks to David Becerra-Alonso (Universidad Loyola Andalucía, Spain) for a critical reading of the manuscript. LMP and DL acknowledge partial financial support from FONDECYT1180905. DL acknowledges partial financial support from Centers of excellence with BASAL/CONICYT financing, Grant AFB180001, CEDENNA.

References

[1] P. Harrison, A. Valavanis, Quantum Wells, Wires and Dots: Theoretical and Computational Physics of Semiconductor Nanostructures, 4th ed., Wiley, 2016.
[2] X. Lan, M. Chen, M.H. Hudson, V. Kamysbayev, Y. Wang, P. Guyot-Sionnest, D.V. Talapin, Nat. Mater. 1 (2020) 7.
[3] S. Pradhan, F. Di Stasio, Y. Bi, S. Gupta, S. Christodoulou, A. Stavrinadis, G. Konstantatos, Nat. Nanotechnol. 14 (2019) 72.
[4] G. Azzellino, F.S. Freyria, M. Nasilowski, M.G. Bawendi, V. Bulovic, Adv. Mater. Technol. 4 (2019) 1800727.
[5] Y.M. El-Batawy, A. Hosny, Opt. Quant. Electron. 52 (2020) 60.
[6] S. Nasa, S.P. Purohit, Physica E 118 (2020) 113913.
[7] B. Çakır, Y. Yakar, A. Özmen, Philos. Mag. 100 (2020) 248.
[8] B. Zhu, F. Wang, C. Liao, H. Zhang, J. Zhang, Y. Cui, Y. Ye, Y. Gu, Opt. Express 27 (2019) 1777.
[9] S. Baskoutas, E. Paspalakis, A.F. Terzis, Phys. Rev. B 74 (2006) 153306.
[10] I. Karabulut, S. Baskoutas, J. Appl. Phys. 103 (2008) 073512.
[11] Z.H. Zhang, K.X. Guo, B. Chen, R.Z. Wang, M.W. Kang, S. Shao, Superlatt. Microstruct. 47 (2010) 325.
[12] R. Khordad, H. Bahramiyan, Superlatt. Microstruct. 76 (2014) 163.
[13] A.J. Peter, Physica E 28 (2005) 225.
[14] D. Bejan, E.C. Niculescu, Eur. Phys. J. B 89 (2016) 138.
[15] W. Xie, Phys. B: Condens. Matter 405 (16) (2010) 3436.
[16] J.W. Robinson, J.H. Rice, K.H. Lee, J.H. Na, R.A. Tay, Appl. Phys. Lett. 86 (2005) 213103.
[17] B. Li, K.-X. Guo, Z.-L. Liu, Y.-B. Zheng, Phys. Lett. A 372 (2008) 1337.
[18] R. Khordad, H. Bahramiyan, Opt. Spectrosc. 117 (2014) 447.
[19] Y.B. Yu, H.J. Wang, Superlatt. Microstruct. 50 (2011) 252.
[20] S. Shojaei, A. Soltani Vala, Physica E 70 (2015) 108.
[21] G. Liu, K. Guo, H. Hassanabadi, L. Lu, Physica B 407 (2012) 3676.
[22] M.K. Bahar, A. Soylu, Phys. Plasmas 25 (2018) 022106.
[23] M.K. Bahar, A. Soylu, J. Phys. B: At. Mol. Opt. Phys. 51 (2018) 105701.
[24] Y.P. Varshni, Superlatt. Microstruct. 30 (2001) 45.
[25] W. Xie, Opt. Commun. 283 (2010) 3703.
[26] B. Vaseghi, M. Sadri, G. Rezaei, A. Gharaati, Physica B 457 (2015) 212.
[27] D. Bejan, E.C. Niculescu, Philos. Mag. 96 (2016) 1131.
[28] M.K. Bahar, A. Soylu, Phys. Plasmas 25 (2018) 062113.
[29] M.K. Bahar, A. Soylu, IEEE Trans. Plasma Sci. 40 (2019) 1713.
[30] P.M. Morse, Phys. Rev. 34 (1929) 57.
[31] S. Sakiroglu, E. Kasapoglu, R.L. Restrepo, C.A. Duque, I. Sökmen, Phys. Status Solidi 254 (2016) 1600457.
[32] M.G. Barseghyan, A.A. Kirakosyan, D. Laroze, Opt. Commun. 383 (2017) 571.
[33] J.H. Davies, The Physics of Low-Dimensional Semiconductors: An Introduction, Cambridge University Press, Cambridge, 1999.
[34] J.C. Martinez-Orozco, F. Ungan, K.A. Rodriguez-Magdaleno, Phys. Scr. 95 (2020) 035802.
[35] A. Radu, A.A. Kirakosyan, D. Laroze, M.G. Barseghyan, Semicond. Sci. Technol. 30 (2015) 045006.
[36] H.M. Baghramyan, M.G. Barseghyan, A.A. Kirakosyan, J.H. Ojeda, J. Bragard, D. Laroze, Sci. Rep. 8 (2018) 6145.
[37] T. Chakraborty, A. Manaselyan, M. Barseghyan, D. Laroze, Phys. Rev. B 97 (2018) 041304(R).
[38] T.G. Emam, Can. J. Phys. 87 (2009) 1159.
[39] J.W. Brown, H.N. Spector, J. Appl. Phys. 59 (1986) 1179.
[40] F. Ungan, M.E. Mora-Ramos, M.G. Barseghyan, L.M. Pérez, D. Laroze, Physica E 114 (2019) 113647.
[41] I. Karabulut, Ü Atav, H. Şafak, M. Tomak, Eur. Phys. J. B 55 (2007) 283.
[42] F. Ungan, J.C. Martínez-Orozco, R.L. Restrepo, M.E. Mora-Ramos, Optik 185 (2019) 881.
[43] F. Ungan, S. Pal, M.E. Mora-Ramos, J.C. Martínez-Orozco, Optik 188 (2019) 12.